JOURNAL OF ATMOSPHERIC AND OCEANIC TECHNOLOGY

# Turbulence measurements from velocimeters on compliant mid-water moorings

LEVI KILCHER*, JIM THOMSON, SAMUEL HARDING AND SVEN NYLUND

ABSTRACT

THE ABSTRACT.

## 1. Introduction

- History of ADVs
- Discussion of ADV v. ADP measurement
- ADVs have been difficult to deploy at mid-depths
- Availability of cheap+accurate IMUs (from smartphone tech) facilitates a new era of ADV measurement from moored platforms.
- Emphasize noise issue and spatial smearing of ADPs.

## 2. Measurements

This work is focused on measuring turbulence spectra from moored ADVs that are equipped with inertial motion sensors (IMU). The ADVs utilized for these measurements were all equipped with Microstrain 3DM-GX3-25 IMU sensors that captured all 6 components of the ADV motion (3 components of angular rotation and 3 components of linear acceleration), as well the orientation of the ADV pressure-case. The sampling of the motion sensor is tightly synchronized with the ADV measurements. The IMU measures its motion at 1kHz and uses internal signal integration (Kalman filtering) to output the motion signals at the same sample rate as the ADV's velocity measurements. This reduces aliasing of the IMU's motion measurements above the ADV's sample-rate (MicroStrain 2010).

### *a. Measurements*

This work utilizes data from two distinct mooring systems to demonstrate the advantages and limitations of each platform. Both mooring systems were deployed in Admiralty Inlet, Washington, approximately 500 meters (m) WSW of Admiralty Head–Fort Casey State Park–in 60 m of water depth at latitude 48.153 north and longitude 122.687 west (Figure 1). The site is approximately 6 kilometers (km) east of Port Townsend, and 1 km north of the Port Townsend – Coupeville ferry route. Admiralty inlet is the largest waterway connecting Puget Sound to the Strait of Juan de Fuca, and it possesses a large semi-diurnal tidal flow.

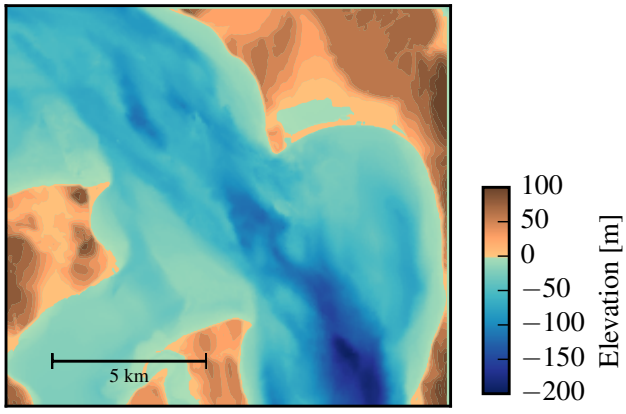


FIG. 1. Bathymetry of Admiralty Inlet at Admiralty Head.

#### 1) TIDAL TURBULENCE MOORING (TTM)

The 'Tidal Turbulence Mooring' (TTM) is a simple mooring system with a 'strongback fin' suspended between a steel clump-weight anchor weighing 1200 kilograms (kg, dry) and a 0.93 m-diameter spherical steel buoy with a buoyancy of 320 kg . The ADV pressure cases were clamped to one side of a 'strongback' fin and the ADV sensor head was positioned 10cm in front of the fin's leading edge (Figure 2). The leading edge of the fin is fastened inline with the mooring line. This configuration was designed to work similar to a weather-vane, such that the drag on the fin held the ADV head upstream of the mooring components. This work utilizes data from two TTM deployments.

*Corresponding author address: National Renewable Energy Laboratory, Golden, Colorado
E-mail: Levi.Kilcher@nrel.gov

The first was in June of 2012 at 48.15285 north, 122.68581 west, near Admiralty Head in Puget Sound, Washington (USA). The mooring was in the water from 17:30 on the 12th until 14:30 on the 14th (local time). Two Nortek ADVs were clamped to either side of the fin such that the axis of their cylindrical pressure-cases were parallel with the leading edge of the strongback. Only one of these ADVs was equipped with an integrated IMU. This TTM also had an upward-looking acoustic Doppler profiler mounted on the mooring anchor.

Periods of time during which this mooring interfered with a beam of the Doppler profiler were identified by inspection of the profiler's acoustic amplitude signal. Periods during which one beam of the profiler had $> 5\%$ higher acoustic amplitude than the other beams were flagged as 'contaminated' and excluded from averaging. 5-minute averages in which more than 50% of the data was contaminated in this way are not shown.

The second TTM deployment was in 2014 from 06:00 on June 17 to 05:00 on June 19. The mooring was positioned at 48.15327 north, 122.68654 west. Two Nortek ADV-IMUs were mounted on this TTM. In this case the pressure-cases and ADV heads were inclined at an angle of 18° to the leading edge of the fin to account for mooring blow-down during strong currents (Figure 3). This change reduced vibrational motion believed to be associated with vortex shedding from the ADV pressure cases when they are oriented cross-wise to the flow (as in the June 2012 deployment).

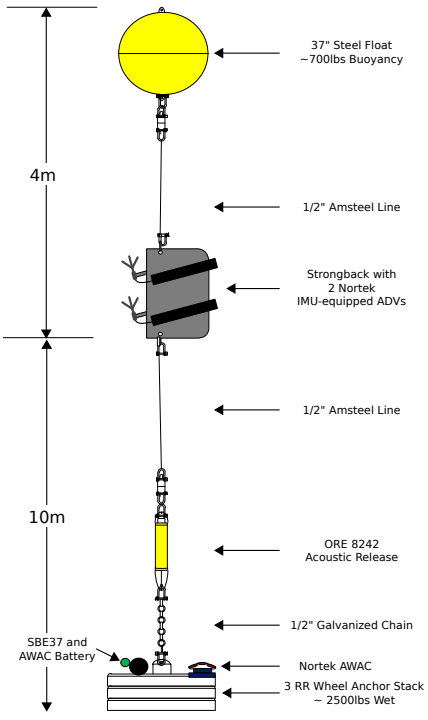


FIG. 2. Schematic diagram of the TTM, not to scale.

FIG. 3. TTM components on the deck of the R/V Jack Robertson. The TTM includes two ADVs, with pressure-cases mounted on opposite sides of the fin. The anchor stack includes a pop-up buoy for retrieval.

### 2) STABLEMOOR

The second mooring system was a cylindrical syntactic foam buoy (manufacturer: Deep Water Buoyancy) that was anchored to a clump weight that weighed 2700 lbs (Figure 4). The buoy is 3.5 m long and 0.45 m in diameter with a tail ring that is 0.76 m in diameter. The buoy was deployed from 11:21 on May 11, 2016 to 12:00 on May 12, 2016 at 48.15277 north, 122.68623 west.

The StableMoor platform has two primary advantages compared to the TTM. First, it is significantly more massive and hydro-dynamically stable than the TTM, which reduces the frequency of motions of the platform. The other major advantage of the StableMoor platform is that it is capable of supporting an acoustic Doppler profiler that provides an independent measure of the platform's translational motion by bottom-tracking. The disadvantages of the Stable Moor is that its size introduces new challenges in deployment and recovery, and it is significantly more expensive than the TTM system.

The StableMoor weighs 295 kg in air, and has a buoyancy of 185 kg in water. An ADV head was positioned 0.1 m in front of the buoy nose. The buoy was equipped with a 1200 kHz RDI workhorse sentinel acoustic Doppler profiler that was pointed downward and configured to measure water velocity below the platform in 12 1-meter bins and measure buoy motion ('bottom tracking'), all at a 1 Hz sample rate. The bottom track velocity provides an independent measure of platform motion that aids in correcting velocity measurements for mooring motion.

The buoy platform was ballasted to pitch upward a few degrees in zero-flow to avoid 'flying downward'. In the presence of an oncoming current the tail fins help to orient

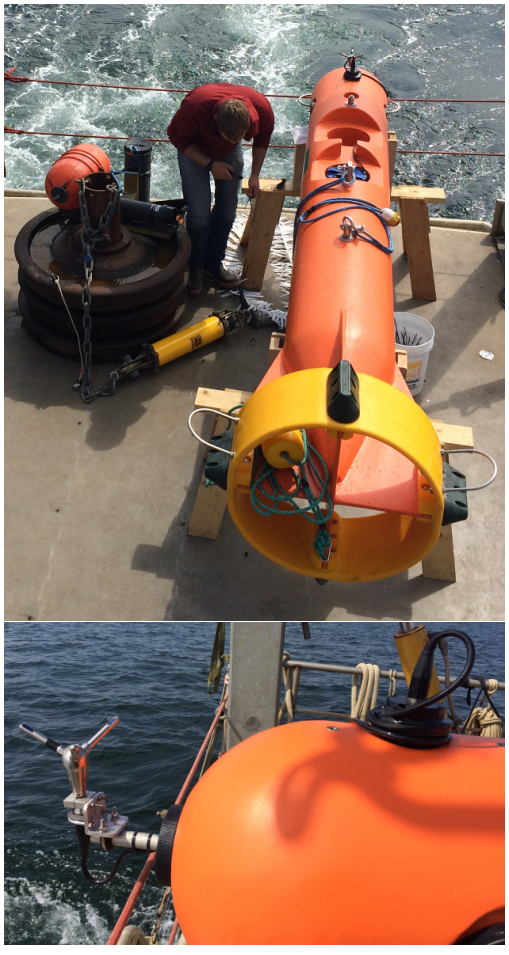

FIG. 4. Alex DeKlerk checks to ensure that the StableMoor buoy is properly fastened to its anchor; the RDI workhorse ADCP can be seen in the rear instrument bay (top). A bridle is draped across the top of the buoy for deployment and recovery, and a small marker buoy fastened to the tail is useful during recovery. A close-up of the StableMoor nose shows the ADV head and the top of its pressure case (bottom).

it into the flow. The anchor for this buoy is similar to that of the TTM, including an acoustic release so the mooring and anchor can be recovered separately. Additional details, photos, and schematic diagrams of both mooring systems are available in Harding et al. (2016).

### *b. Principal-axes coordinate system and turbulence averaging*

Unless stated otherwise, vector quantities in this work are in a fixed 'principal-axes' coordinate system that is aligned with the bi-directional tidal flow: positive $u$ is in the direction of ebb (310° True), positive $w$ is vertically upward, and $v$ is the cross-stream component in a right-handed coordinate system. The full velocity vector, $\vec{\tilde{u}} = (\tilde{u}, \tilde{v}, \tilde{w})$, is separated into a mean and turbulent component as $\vec{\tilde{u}} = \vec{\bar{u}} + \vec{u}$, where the over-bar denotes a 5 minute average. Throughout this work we use $\bar{U} = (\bar{u}^2 + \bar{v}^2)^{1/2}$ to denote the horizontal velocity magnitude.

All spectra and cross-spectra are computed as the variance preserving squared magnitude of the Fourier transform using standardized (NumPy) fast Fourier transform routines (i.e. $\int S\{u\}\mathrm{d}f = \overline{u^2}$). Time series' are linearly detrended and Hanning windowed prior to computing the Fourier transform to reduce spectral reddening. Turbulence dissipation rates are computed as,

$$\varepsilon = \frac{1}{\bar{U}} \left( \alpha \left\langle (S(u) + S(v) + S(w)) f^{5/3} \right\rangle_{f_{IS}} \right)^{3/2} \tag{1}$$

Where $\alpha = 0.5$, and $\langle\rangle_{f_{IS}}$ denotes an average over the inertial-subrange of the velocity spectra and where the signal-to-noise ratio is small (Lumley and Terray 1983; Sreenivasan 1995). Throughout this work we take this average from 0.3 to 1 Hz for the $u$ and $v$ components, and 0.3 to 3 Hz for the $w$ component.

## 3. Methodology

The essential approach of this methodology is to estimate time-series of velocity on a compliant mooring by obtaining an independent estimate of ADV head motion and removing that motion from the measured signal. Nortek offers an ADV that is equipped with an IMU that measures the linear acceleration, rotational-motion, and orientation of the ADV pressure case (body). So long as the ADV head is rigidly connected to the ADV pressure case, it is possible to utilize the IMU motion signals to calculate the motion of the ADV head, and remove it from the measured velocity signal. The ADV head motion, is calculated as the sum of rotational and translational motion, which are each estimated from the IMU's angular-rate, $\vec{\omega}$, and acceleration, $\vec{a}$, signals as:

$$\vec{u}_{\mathrm{h}} = \vec{u}_{\omega} + \vec{u}_{a} + \vec{u}_{\mathrm{low}} \tag{2}$$

$$= \mathbf{R}^{\mathrm{T}} \cdot \vec{\omega}^{*}(t) \times \vec{\ell}^{*} + \int \{\vec{a}(t)\}_{HP(f_a)} \mathrm{d}t + \vec{u}_{\mathrm{low}} \tag{3}$$

Here '$*$' superscripts denote quantities in the ADV's locale coordinate system, $\mathbf{R}^{\mathrm{T}}$ is the IMU orientation matrix that rotates vectors from the IMU to the earth reference frame, and $\vec{\ell}^{*}$ is the vector from the IMU to the ADV head. The notation $\{\vec{a}\}_{HP(f_a)}$ indicates that the IMU's accelerometer signal is high-pass filtered (in the earth's stationary reference frame) at a chosen filter-frequency, $f_a$. This is necessary because accelerometers have low-frequency noise, sometimes referred to as 'bias-drift' (NEED CITATION for: Accelerometer noise). This noise is amplified by integration of the acceleration signal such that it contaminates the motion correction, especially at low-frequencies (Figure 3). This issue means that low-frequency motion is not well resolved by the IMU, and so there is a residual

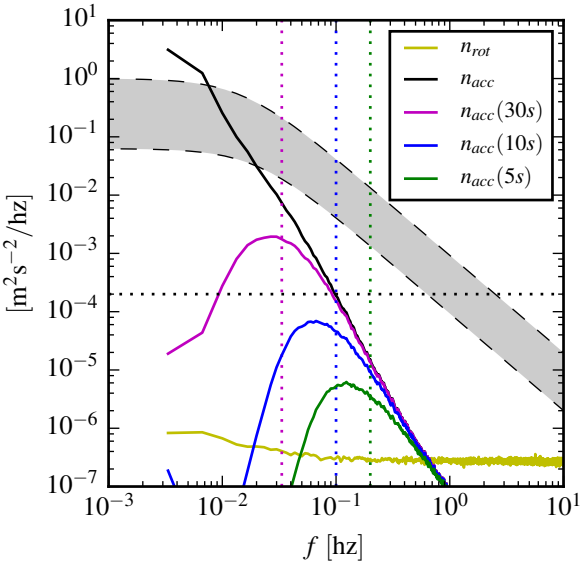


FIG. 5. Spectra of $\vec{u}_\omega$ (yellow) and $\vec{u}_a$ signals from the Microstrain IMU sitting on a motionless table. The $\vec{u}_a$ signals are unfiltered (black), and high-pass filtered at 30s (magenta), 10s (blue), 5s (green). Vertical dotted lines indicate the filter frequency. The black horizontal dotted line indicates the noise-level of a Nortek Vector ADV configured to measure ±4m/s. The shaded region indicates the range of spectra presented herein ($0.002 < \text{tke} < 0.03\ \text{m}^2/\text{s}^2$, 1e-5 $< \varepsilon <$ 5e-4 W/kg).

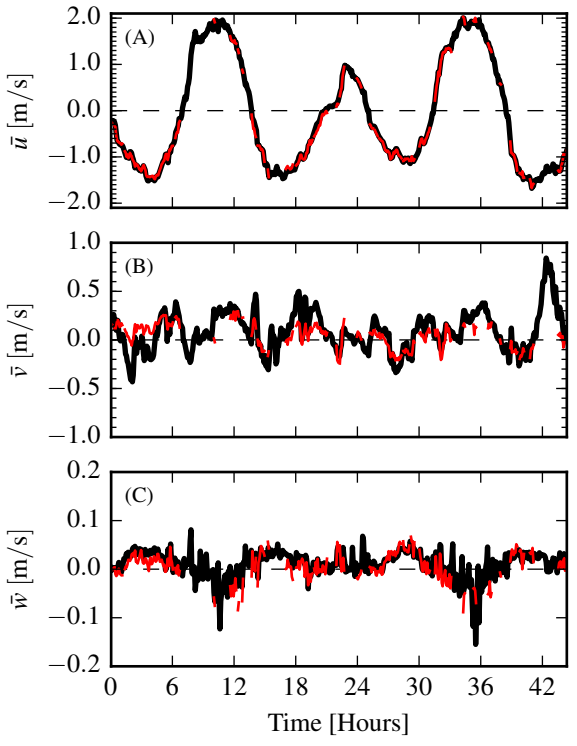


FIG. 6. Time series of tidal velocity at Admiralty Head from TTM measurements (black), and an acoustic Doppler profiler (red). The profiler measurements–taken at the same depth as the ADV on the TTM—were contaminated by acoustic reflection from the strongback fin when it was inline with one of the profiler's beams. Note that the vertical scale on the three axes vary by more than an order of magnitude; the small ticks in A and B are equivalent to the ticks in C.

low-frequency translational motion, $\vec{u}_{\text{low}}$, that needs to be considered when performing motion correction.

For the TTM we utilize $f_a = 0.0333Hz$ (30 second period), and assume that $\vec{u}_{\text{low}} = 0$. For the StableMoor $f_a = 0.2Hz$ (5 second period). The bottom-track velocity was low-pass filtered at this frequency to provide an estimate of $\vec{u}_{\text{low}}$, and $\vec{a}$ was high-pass filtered at this frequency. We use 4-pole, bi-directional (zero-phase), Hanning filters for all filtering operations.

The choice of high-pass filter to be used to correct for low-frequency accelerometer noise issue depends on the application (e.g. deployment platform), and the turbulence level of the measurement environment. In particular, this involves a trade off between filtering-out this noise and not filtering measured motion (Figure 3). If an independent measure of low-frequency motion is available, it is possible to combine that signal with the IMU's high-frequency motion measurements to obtain a complete estimate of ADV motion. Lacking an independent measure of low-f motion, the user may instead choose to neglect the portion of the spectrum below the filter frequency, or demonstrate that platform motion at those frequencies is small compared to the measured signal based on other considerations.

With this estimate of ADV head motion it is straightforward to correct the measured velocity, $\vec{u}_{\text{m}}$, to estimate the velocity in the earth's inertial reference frame:

$$\vec{u}(t) = \vec{u}_{\text{m}}(t) + \vec{u}_{\text{h}}(t) \quad . \tag{4}$$

Note here that the '+'-sign is correct because head motion, $\vec{u}_{\text{h}}$, induces a measured velocity in the opposite direction of the head motion itself ($\vec{u}_{\text{m}} = \vec{u} - \vec{u}_{\text{h}}$).

Additional details on motion correction–including a detailed accounting of the distinct coordinate systems of the IMU, ADV pressure case, and ADV head–can be found in Kilcher et al. (2016). Open-source Python tools for performing motion correction of ADV-IMU data–including scripts that write processed data in Matlab and tabulated formats–are available at `http://lkilcher.github.io/dolfyn/`.

## 4. Results

### *a. Mean velocity*

A comparison of mean velocity measured by an ADV-IMU mounted on a TTM, to that of an upward-looking acoustic Doppler profiler mounted on the TTM anchor

is presented in Figure 6. This shows excellent agreement between the ADV and Doppler profiler measurements of velocity. The $u$, $v$ and $w$ components have a root-mean-square error of 0.05, 0.13 and 0.03 m/s, respectively. While it is important to note that their is some discrepancy between ADP and ADV measured velocities (especially in the $v$-component, which is most likely due to incomplete motion correction), the agreement between the magnitude and direction of these independent velocity measurements indicates that moored ADV-IMUs provide a reliable estimate of velocity in the Earth's reference frame.

### b. TTM Spectra

As discussed in detail in the companion paper, the mooring motion of the TTM, $S\{\vec{u}_{\rm h}\}$, has a peak at 0.1 to 0.2 Hz from swaying of the mooring that is most likely driven by eddy-shedding from the spherical buoy (Figure 7, red lines). There is also broad-band motion that is associated with fluttering of the strongback fin around the mooring line. Both of these motions are especially energetic in the $v$-component spectra, because this is the direction in-which the TTM mooring system is most unstable. As is expected from fluid-structure interaction theory the amplitude of these motions increases with increasing mean velocity (Morison et al. 1950).

The mooring motion contaminates the uncorrected ADV-measurements of velocity, $S\{\vec{u}_{\rm m}\}$, whenever the amplitude of the motion is similar to or greater than the amplitude of the turbulence. Fortunately, much of this motion can be removed using the IMU's motion signals as detailed in section 3. Lacking an independent measurement of turbulence velocity at this site, we interpret the agreement of these spectra with turbulence theory as evidence of the success of the method. In particular, for each mean-flow speed the spectra decay with a $f^{-5/3}$ slope and have equal amplitude across the velocity components. These results are consistent with Kolmogorov's (1941) theory of isotropic turbulence, and are consistent with other measurements of turbulence in energetic tidal channels from stationary platforms (Kolmogorov 1941; Walter et al. 2011; Thomson et al. 2012; McMillan et al. 2016).

As successful as motion correction is, some of the motion contamination persists in $S\{\vec{u}\}$. This is most notable in the $v$-component spectra at the highest flow speeds where a peak in $S\{v\}$ at 0.15 Hz is nearly an order of magnitude larger than a typical turbulence spectral fit to the other frequencies would indicate. This persistent motion contamination is evident to a lesser degree in the $u$-component spectra at the highest flow speed, and in the $v$-component spectra at lower flow speeds. The $w$-component spectra appear to have no persistent motion contamination. This is largely because the amplitude of the motion in this direction is much lower than for the other two components. In fact, for these measurements, the $w$-component of mooring motion is so low that $w$-component motion correction is significant only at the highest flow speeds (i.e. motion correction removes the 0.15 Hz peak).

The amplitude of the persistent motion contamination peaks at 0.15 Hz are a factor of 5 to 10 times smaller than the amplitude of the ADV head motion itself. This suggests the Microstrain IMU's motion signals can be used to effectively correct for mooring motion at 0.15 Hz when the amplitude of that motion is less than 5 times the amplitude of the real turbulence spectrum.

This reveals an ancillary benefit of the IMU measurements, which is that they can assist with identifying and accounting for persistent sources of motion contamination. For example, one of the most common uses of turbulence spectra is for the calculation of the turbulent kinetic energy dissipation rate, $\varepsilon$, or for calculating the total turbulent kinetic energy, tke. In particular, the regions of the spectrum where the motion is a factor of 3 to 5 larger than the measured signal can be excluded from a spectral fit. The fit can the be used to estimate tke and $\varepsilon$.

### c. StableMoor Spectra

The spectra of the stablemoor motion has a broader peak with a maximum amplitude that is at approximately half the frequency of the TTM spectral peak (Figure 8). The motion of this platform also does not have high-frequency 'sub-peaks' or other high-frequency broad-banded excitation. These characteristics of the motion are most-likely due to the more massive and hydrodynamically streamlined nature of the platform.

Like the TTM, the motion-corrected spectra from the StableMoor are consistent with turbulence theory and previous observations. Most importantly, there is an improvement in the quality of the motion corrected spectra compared to the TTM. In particular their does not appear to be significant persistent motion contamination peaks in these spectra. When the assumption that $\vec{u}_{\rm low} = 0$ is made, peaks and troughs are seen in the data, which suggests that the improvement in motion correction is largely the result of an accurate measurement of $\vec{u}_{\rm low}$.

### d. Torpedo Spectra

### e. Reynold's stresses

## 5. Discussion

For many applications, such as estimating the turbulence dissipation rate, or turbulent kinetic energy, estimating the spectra is an intermediate step...

- Compare the motion correction of SM to TTM: SM does better because it is more stable, and has a measurement of $u_{\rm low}$. Discuss spectral coherence of $u_{\rm BT}$

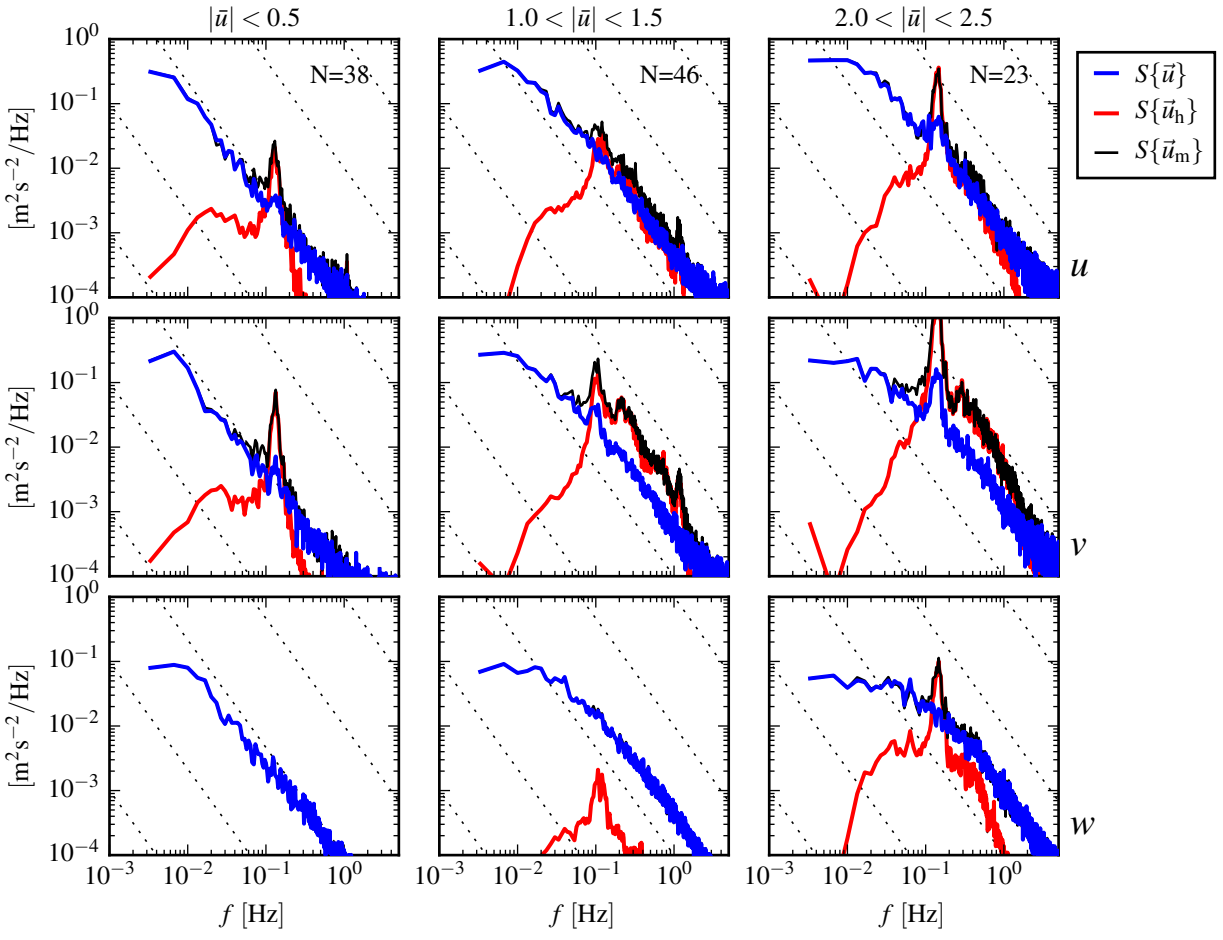


FIG. 7. Turbulence spectra from the TTM for 3 ranges of mean stream-wise velocity (first column: $|u| < 0.5$ m/s, second column: $1 < |u| < 1.5$ m/s, third column: $2 < |u| < 2.5$ m/s). The rows are for each component of velocity (top: $u$, middle: $v$, bottom: $w$). The uncorrected spectra are in black and the corrected spectra are blue. The spectra of ADV head motion, $\vec{u}_h$, is red. Diagonal dotted-lines indicate a $f^{-5/3}$ slope. N is the number of spectral-ensembles in each column.

with IMU, i.e. Figure 15. This is important because it shows the low-$f$ limit of the IMU measured motion.

- $\vec{u}_h$ provides a justification, and a screening criteria(?), for removing portions of the signal.
- Can estimate $\varepsilon$, tke with fits that exclude contaminated portions of the spectra.
- Can remove up to 10x signal motion
- Discuss the time-domain method vs. spectral (cross-coherence) methods, and the need for phase information.
- Should we estimate $\varepsilon$ in this paper? If so, should this be in the Results section?

## 6. Conclusion

*Acknowledgments.* Many thanks to Joe Talbert, Alex DeKlerk, Captain Andy Reay-Ellers, Maricarmen Guerra, Marshall Richmond, James VanZwieten, Matthew Egeland and Jennifer Rinker.

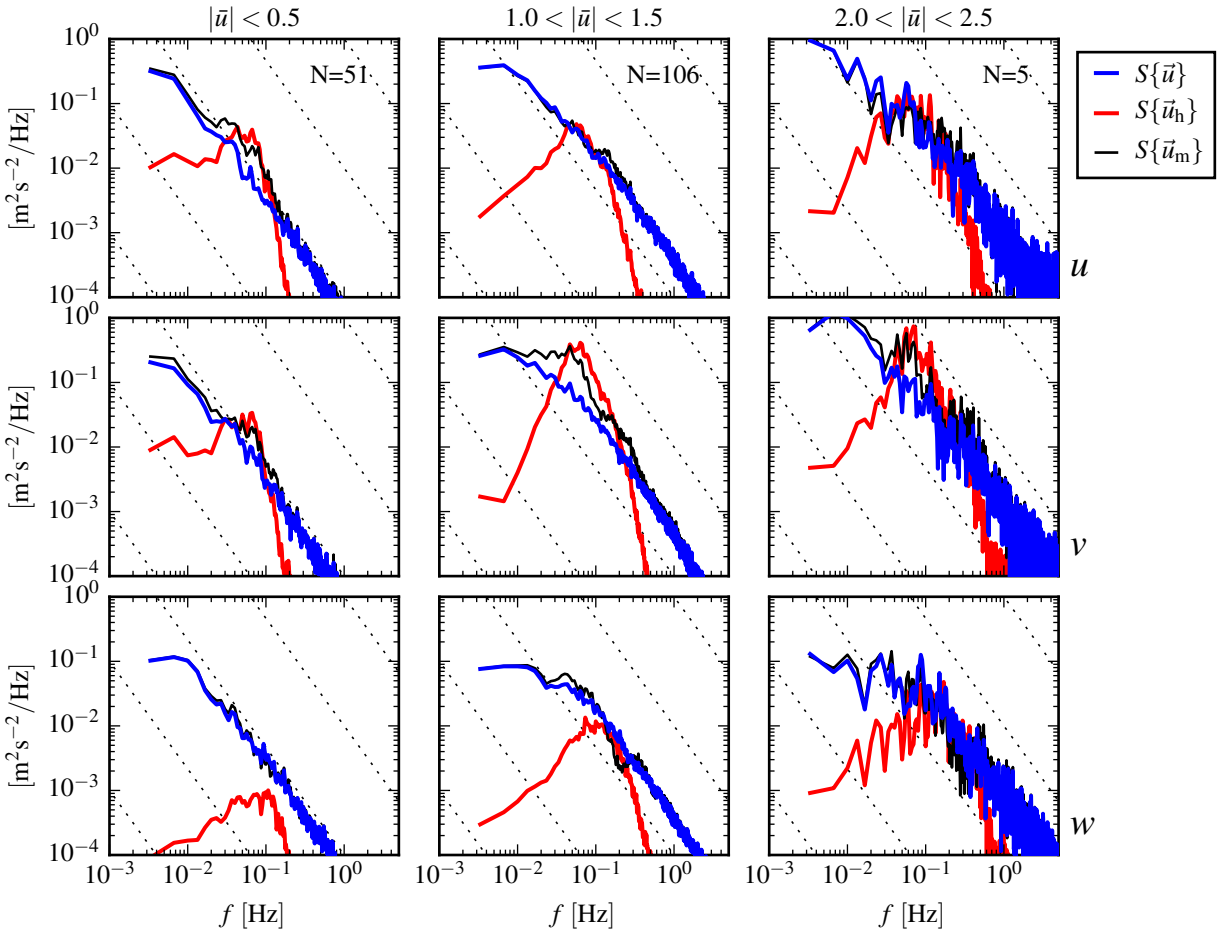


FIG. 8. Turbulence spectra from the StableMoor buoy. The axes-layout and annotations are identical to Figure 7.

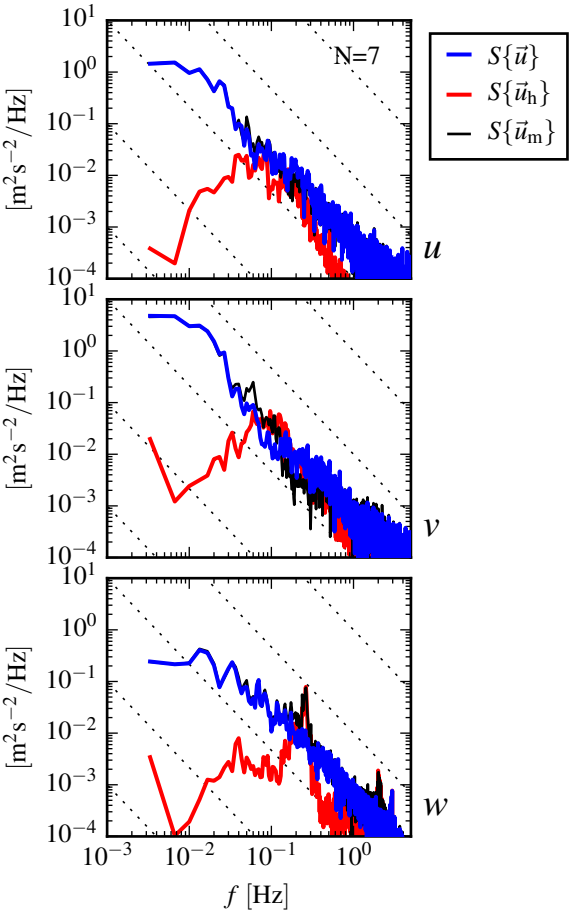


FIG. 9. Turbulence spectra from the turbulence torpedo during a 35 minute period when the mean velocity was 1.3 m/s. Annotations and line colors are identical to Figure 7.

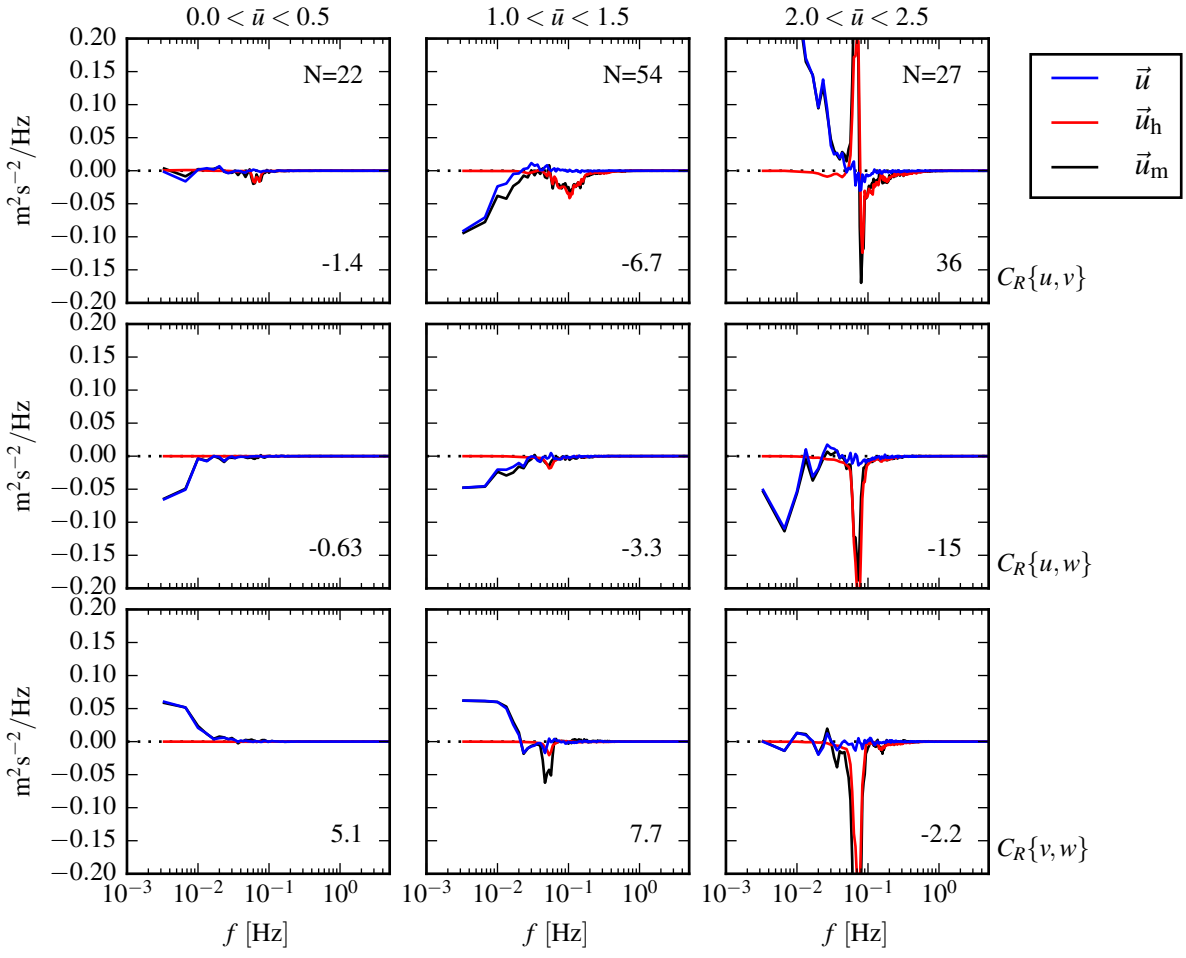


FIG. 10. The real part of the cross-spectral density between velocity components measured by the TTM. The upper-row is the *u*-*v* cross-spectral density, the middle-row is the *u*-*w* cross-spectral density, and the bottom-row is the *v*-*w* cross-spectral density. The columns are for different ranges of the stream-wise mean velocity magnitude. The blue line is the cross-spectrum between components of motion-corrected velocity, the red line is the cross-spectrum between components of head-motion, and the black line is the cross-spectrum between components of uncorrected velocity. N is the number of spectral ensembles in each column. The number in the lower right corner of each panel is the motion-corrected Reynold's stress (integral of the blue line) in units of 1e-4 $m^2s^{-2}$.

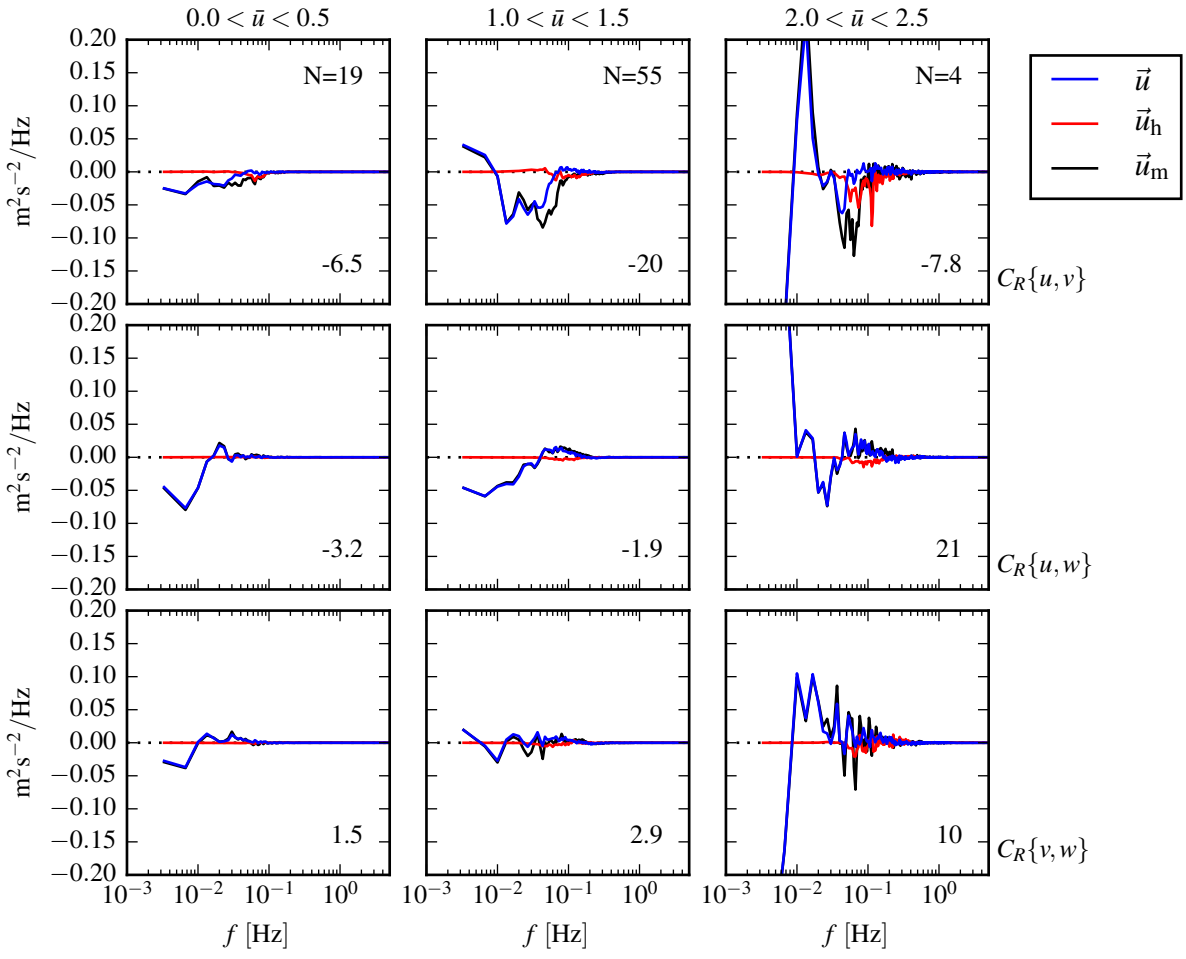


FIG. 11. The real part of the cross-spectral density between velocity components measured by the StableMoor buoy. The axes-layout and annotations are identical to Figure 10.

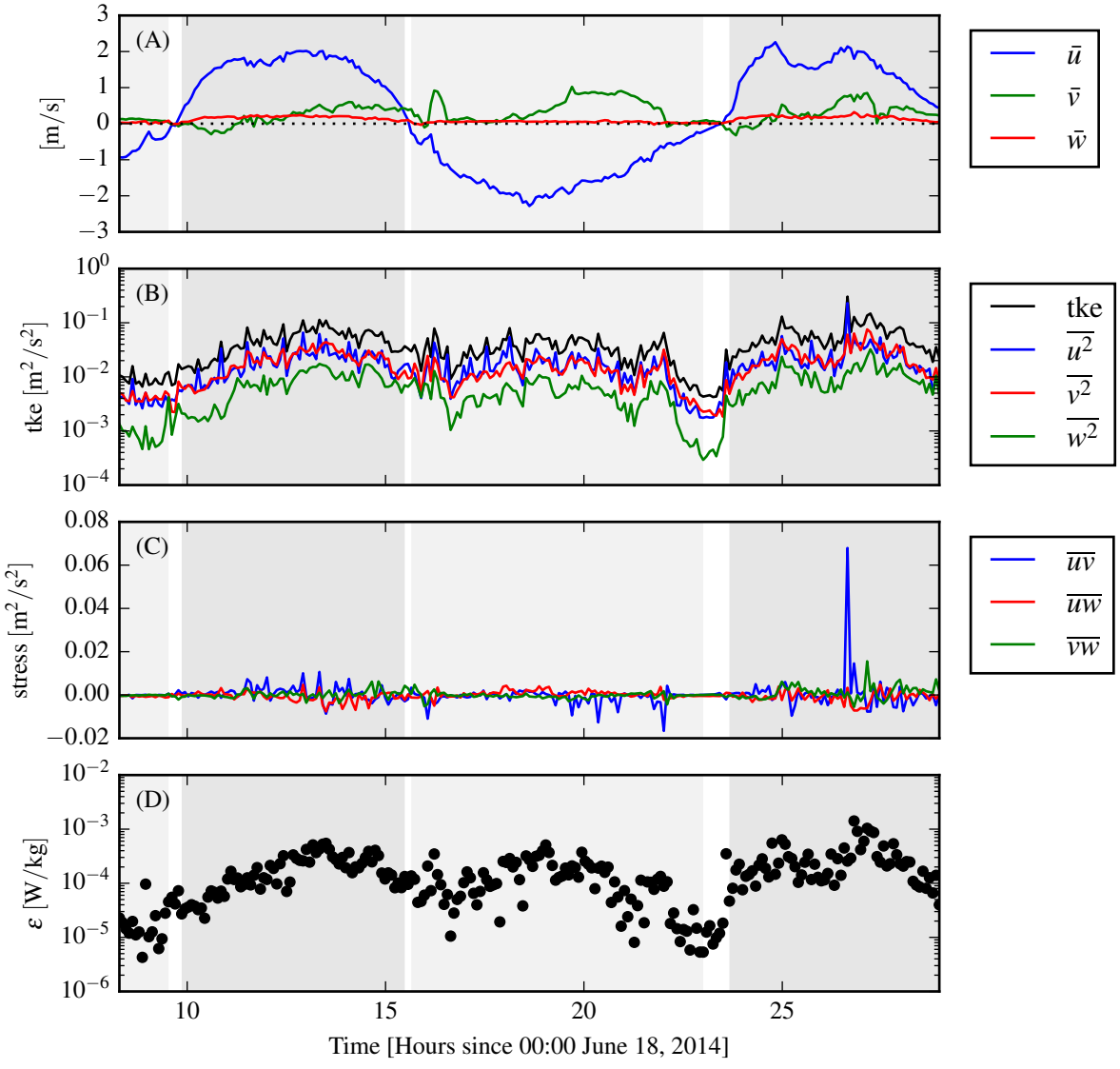


FIG. 12. Time-series of mean velocities (A), turbulence energy and its components (B), Reynold's stresses (C), and turbulence dissipation rate (D) measured by the TTM during the June, 2014 deployment. Shading indicates periods of ebb ($\bar{u} > 0.2$, grey), and flood ($\bar{u} < -0.2$, lighter grey).

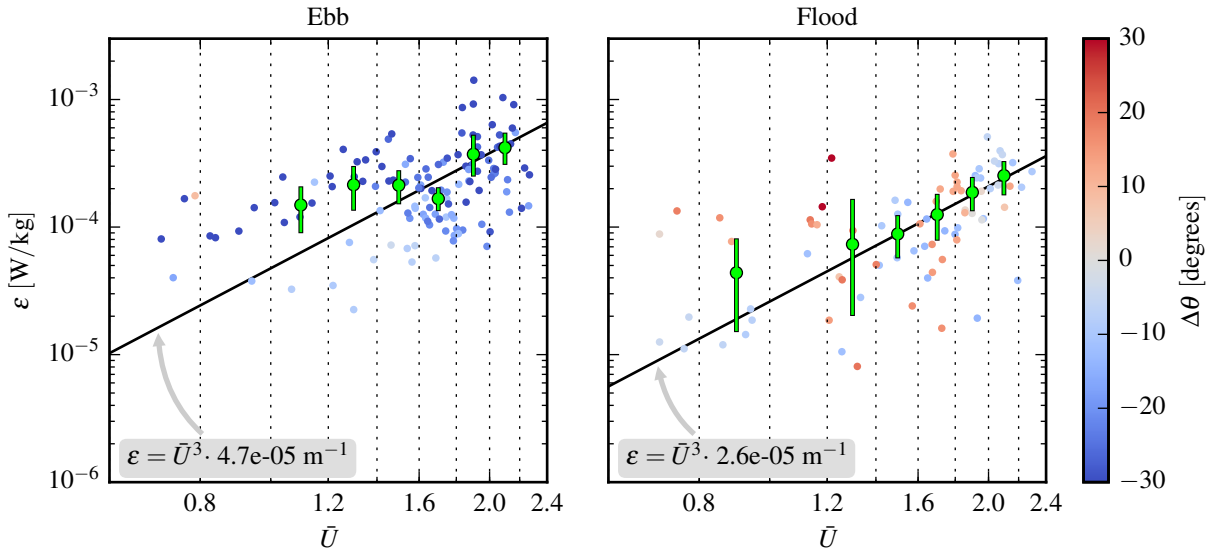


FIG. 13. $\varepsilon$ versus $\bar{U}$ for the June 2014 TTM deployment during ebb (left), and flood (right). Small points are 5 minute averages, and their color indicates the angle of the mean horizontal velocity relative to the principal ebb or flood direction ($\Delta\theta = \theta - \theta_\circ$, where $\theta$ is the horizontal velocity direction, and $\theta_\circ$ is 310° and 130° true for ebb and flood, respectively). Green dots are mean values within speed bins of 0.2 m s$^{-1}$ width that have at least 6 points (30 minutes of data); their vertical bars are 95% bootstrap confidence intervals. The black line shows a $U^3$ slope, where the proportionality constant (grey box) is calculated by taking the log-space mean of $\varepsilon/U^3$.

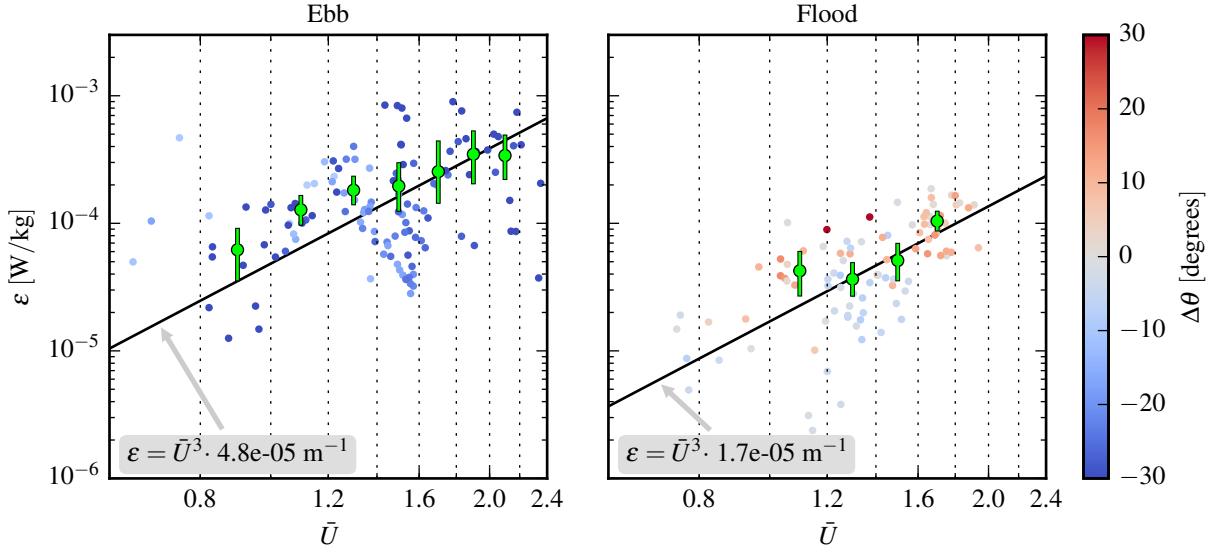


FIG. 14. $\varepsilon$ versus $\bar{U}$ for the May 2015 StableMoor deployment during ebb (left), and flood (right). The markers and annotations are identical to figure 13.

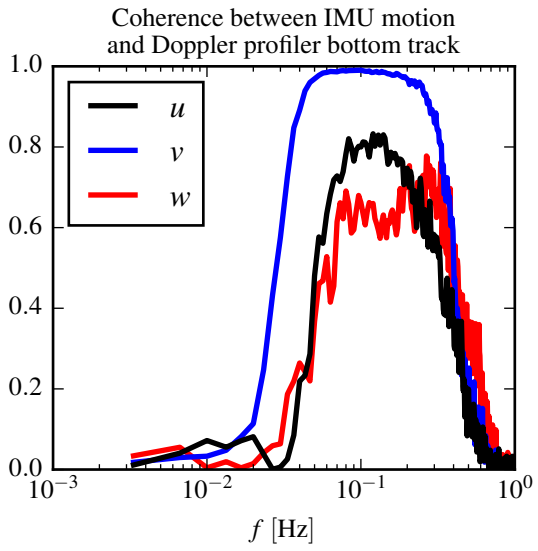


FIG. 15. Coherence between stablemoor IMU measured motion and bottom track velocity.

## References

Harding, S., L. Kilcher, and J. Thomson, 2016: Motion of tethered instrument platforms for acoustic doppler velocimetry in energetic tidal flows, simul-pub?

Kilcher, L., J. Thomson, J. Talbert, and A. DeKlerk, 2016: Measuring turbulence from moored acoustic Doppler velocimeters: A manual to quantifying inflow at tidal energy sites. Tech. Rep. 62979, National Renewable Energy Laboratory. URL www.nrel.gov/docs/fy16osti/62979.pdf.

Kolmogorov, A. N., 1941: Dissipation of energy in the locally isotropic turbulence. *Dokl. Akad. Nauk SSSR*, **32 (1)**, 16–18, URL http://www.jstor.org/stable/51981.

Lumley, J., and E. Terray, 1983: Kinematics of turbulence convected by a random wave field. *Journal of Physical Oceanography*, **13 (11)**, 2000–2007.

McMillan, J. M., A. E. Hay, R. G. Lueck, and F. Wolk, 2016: Rates of dissipation of turbulent kinetic energy in a high reynolds number tidal channel. *Journal of Atmospheric and Oceanic Technology*, **33 (4)**, 817–837, doi:10.1175/JTECH-D-15-0167.1, URL http://dx.doi.org/10.1175/JTECH-D-15-0167.1, http://dx.doi.org/10.1175/JTECH-D-15-0167.1.

MicroStrain, I., 2010: Technical note: Coning and sculling. Tech. Rep. I0019, MicroStrain. URL http://files.microstrain.com/TN-I0019_3DM-GX3-25__Coning_And_Sculling.pdf.

Morison, J. R., J. W. Johnson, and S. A. Schaaf, 1950: The force exerted by surface waves on piles. *Journal of Petroleum Technology*, **2 (05)**, 149–154.

Sreenivasan, K. R., 1995: On the universality of the Kolmogorov constant. *Physics of Fluids*, **7**, 2778–2784.

Thomson, J., B. Polagye, V. Durgesh, and M. Richmond, 2012: Measurements of turbulence at two tidal energy sites in Puget Sound, WA. *Journal of Oceanic Engineering*, **37 (3)**, 363–374, doi:10.1109/JOE.2012.2191656.

Walter, R. K., N. J. Nidzieko, and S. G. Monismith, 2011: Similarity scaling of turbulence spectra and cospectra in a shallow tidal flow. *Journal of Geophysical Research: Oceans*, **116 (C10)**.